On the axial bearing capability of construction steel tube considering the uniform corrosion effect

Huajie Wang[a, b], Zhiwei Zhang[b*], Hongliang Qian [a, b], Gang Song [a, c], Jiangbo Wang [a], & Feng Fan[b]

[a] Department of Civil Engineering, Harbin Institute of Technology, Weihai 264200, China

[b] School of Civil Engineering, Harbin Institute of Technology, Harbin 150000, China

[c] Shandong Tong Yuan Design Group Co., Ltd., Jinan 250000, China

To study the law of corrosion on the mechanical properties of the components used in spatial steel structures and obtain the load-carrying capability of circular steel tubes under varying degrees of corrosion, experiments on a periodic spray have been designed to study the accelerated corrosion and axial loading of tubes without a protective layer. The experiment results show that the yield and ultimate load-carrying capacities of the components are heavily influenced by the corrosion, the latter being more sensitive to corrosion, and that a good functional relationship exists between the weight loss ratio and the load-carrying capability of the corrosive components. In addition, a finite element model of a circular steel tube experiencing corrosion has been established using ANSYS with an equivalent cross-section reduction method to simulate of the experiment results. The simulation results agree well with the experiment results, which effectively indicates that the corrosion of the steel tube components obeys the uniform corrosion law. And the equivalent cross-section reduction method also possesses good reliability. The results of the study provide a technical reference for research on the mechanical properties of larger building components such as circular steel tubes experiencing corrosion.

Keywords: Uniform corrosion, Steel tube, Bearing capacity, Periodic atomising compound experiment, Weight loss rate

1 Introduction

With the extensive application of large-span steel structures in construction projects such as stadiums and airports, an increasing number of durability problems of large-span steel structures are highlighted during the late period of their designed lifetime[1-3]. Thus, research into the mechanical properties of a steel construction undergoing corrosion makes significant sense. As for previous studies, Lee and Cho[4] found in their research that the yield strength of steel bars under corrosion increases with an increase in their weight loss rate. Kim *et al.*[5] studied the influence of the local wall thickness on the bearing capacity by comparing a simulation and theoretical calculations. In addition, Flaks designed the exposure experiments for aluminium plates in a natural state, carried out material experiments on the specimens with corrosion, and studied the yield strength, hardness and the damage coefficient of the failure strength[6]. Considering the corrosion effect in light of the thickness reduction, Rahgozar[7] and Sharifi[8] explored both experimentally and theoretically the

mechanical prosperities of an I-shaped steel beam under corrosion. In addition, Val[9] and Stewart[10]analyzed the corrosion states under normal and special environments, respectively, seeking the corrosion effect on the shear resistance and bending strength of the specimens, and calculated their failure probability through the use of Monte Carlo methods. Zhao and Pan studied the flexural rigidity, stability[11], and flexural bearing capacity[12] of a flexural H-steel beam. Additionally, considering the influence of the internal pressure, Teixeira *et al.*[13] and Caleyo *et al.*[14] analysed submarine pipelines and explored the impact of marine corrosion on their reliability and remaining lifetime, respectively. Moreover, Amirat *et al.*[15] studied the effect of residual stress on the reliability of corrosive submarine pipelines. Rajabipour and Melchers analysed the damage to a submarine pipeline under the joint action of pitting corrosion and axial stress through a numerical simulation method[16].

Research on corrosion by, such these scholars has mainly focused on the effects of corrosion on the performance of steel bars and underground energy pipelines. However, there have been few studies on the mechanical properties of circular steel tubes that

---

*Corresponding author (E-mail: 16B933030@hit.edu.cn)

are commonly used in spatial structures. Energy pipelines are mainly concerned with internal pressure, external pressure, bending problems[17-19], whereas the spatial structures are more concerned with axial stress problems[20, 21] and the corrosion forms they face are mainly uniform corrosion. Therefore, it is necessary to study the law of axial force performance after the corrosion of construction steel tubes.

To determine the mechanical properties of corroded circular steel tubes, accelerated corrosion experiments were designed. Meanwhile, as previously mentioned, because axial loading is the most primary type of loading on the specimens used in spatial structures, particularly double-layer reticulated shells and grids, the axial bearing property of corroded steel tubes has been mainly studied using experimental methods. Furthermore, obtaining the law of degradation on the axial bearing of circular steel tubular specimens without a protective layer during the post-corrosion stage would provide theoretical references for the mechanical properties of corrosive circular steel tubes and a safety evaluation of corroded spatial structures.

2 Corrosion Experiments

2.1 Accelerated corrosion test method and design

For a long regular corrosion period, it is difficult to obtain suitable corrosion experiment specimens within a short time frame. To obtain the mechanical properties of corrosive circular steel tubes as quickly as possible, proper accelerated corrosion experiments need to be designed. The experiment material used herein was Q235B mild steel, chemical composition of which is given in Table1.

The traditional indoor accelerated corrosion salt spray experiments are mainly carried out in a salt-fog

chamber. However, owing to both their large size and number architectural circular steel tubes are difficult to place in a salt-fog chamber for indoor accelerating corrosion experiments. Therefore, based on the corrosion principle used in a salt-fog chamber, combined experiments using an outdoor periodic spray satisfying the specimen size requirement and simulating a real outdoor environment have been properly conducted. In addition, the atmospheric corrosion was accelerated under a natural outdoor environment based on the 'wetting-drying' cycles.

The experiment was carried out in an open field with good ventilation and uniform sunshine. The experiment site is located in Weihai, Shandong province, China. All corrosion specimens started outdoor corrosion testing in May-2015. The longest corrosion time was 8 months (to December 2015). The weather data for the Weihai atmospheric corrosion site during this period are summarised in Table 2.

The concentration of hydrochloric acid was 38 %, and uniform spraying on the outer surface of all specimens was conducted once at 18:00 each day.

During the experiments, steel tubes, made from Q235B steel used widely in building construction, were of two specifications, *i.e.* one with an outer diameter of 140 mm and a wall thickness of 3 mm. And the other with an outer diameter of 89 mm and same wall thickness. In addition, the specific sizes of the specimens are listed in Table 3.

During the accelerating corrosion experiments, 'A' stands for the specimens without corrosion, 'B' for those undergoing accelerated corrosion for 10 days, "C" for those undergoing corrosion for 20 days, and 'D' for those undergoing accelerated corrosion for 20 days followed by exposure to an outdoor environment for 5 months. Similar to the arrangement of circular steel tubes with a 140 × 3 section, 'E' indicates exposure in an outdoor environment for 7 months, 'F' for exposure in an outdoor environment for 7 months followed by accelerated corrosion for 20 days, 'G'

Table 1 — Chemical composition of Q235B mild steel (mass %).

C	Mn	Si	S	P	Fe
0.16	0.43	0.18	0.01	0.02	Bal.

Table 2 — Average weather data in Weihai from May to December 2015

Data	Month							
	5	6	7	8	9	10	11	12
Average temperature/℃	18.6	22.2	24.7	26.1	22.4	16.7	8.6	3.5
Average highest temperature/℃	22.7	26.4	28.1	29.3	25.6	20.1	11.1	6.3
Average lowest temperature/℃	14.6	19.1	22.0	23.5	19.6	13.9	6.6	1.3
Precipitation/mm	56.7	23.2	244.6	44.9	15.1	50.7	80.2	12.9
Average relative humidity/%	51.4	68.6	75.7	75.6	67.0	61.1	73.0	65.5
Average wind speed/(m·s⁻¹)	3.7	3.3	2.5	2.4	2.4	3.2	3.5	3.4

Table 3 — Data onthe steel tubes.

Corrosion group	number	Wall thickness/mm	Outer diameter/mm	Length/mm	W_0/g	W_T/g	weight loss /g	D_w	F_{sc}/kN	F_{bc}/kN
	1	2.96	139.4	382.5	3441	3441	0	0	350.0	403.4
A	2	2.98	139.2	380.0	3434	3434	0	0	368.2	412.2
	3	2.93	139.4	377.0	3400	3400	0	0	360.0	416.6
	1	2.99	139.2	387.5	3487	3335	152	4.37%	349.6	388.2
B	2	3.03	139.5	385.5	3469	3293	136	3.92%	363.2	401.6
	3	2.96	139.2	385.5	3475	3283	192	5.52%	356.2	394.2
	1	2.92	139.1	391.5	3531	3379	152	4.30%	355.2	393.4
C	2	2.96	139.3	390.0	3502	3350	152	4.34%	350.2	389.0
	3	2.97	139.3	388.5	3494	3302	192	5.49%	353.6	390.6
	1	2.89	139.1	394.5	3550	2695	855	24.08%	260.2	265.6
D	2	2.95	139.3	393.0	3543	2592	951	26.85%	254.3	271.2
	3	2.99	139.3	392.0	3533	2573	960	27.18%	246.9	263.4
	1	3.01	88.97	310.0	1756	1540	216	12.30%	198.5	245.0
E	2	2.95	89.03	310.0	1761	1553	208	11.82%	196.7	243.2
	3	2.99	88.95	309.5	1755	1491	264	15.04%	187.2	228.8
	1	2.97	89.01	310.0	1760	1488	272	15.46%	169.1	201.4
F	2	2.97	88.89	309.8	1748	1524	224	12.80%	189.5	241.8
	3	2.98	88.89	309.0	1753	1448	305	17.38%	172.3	196.9
	1	3.01	88.95	311.0	1762	1449	313	17.78%	193.8	230.4
G	2	2.96	89.03	309.2	1755	1420	335	19.09%	176.4	204.0
	3	3.02	88.97	309.2	1759	1391	368	20.91%	184.0	210.4
	1	2.96	88.85	309.8	1754	1754	0	0	208.9	281.4
H	2	3.01	88.95	307.9	1751	1751	0	0	212.4	286.6
	3	3.01	89.02	309.8	1766	1766	0	0	212.7	285.8

In the table, F_{sc} represents the yield bearing capacity, and F_{bc} indicates the ultimate bearing capacity.

exposure for 7 months followed by 30 days of accelerated corrosion, and 'H' for no corrosion. Fig. 1 shows a view of the experiment field where the accelerated corrosion experiments were conducted on specimens of groups B, C, and D.

2.2 Experimental phenomena

After accelerated corrosion, both the inner and outer surfaces of the steel tubes show varying degrees of rust layer spalling and an obvious distribution of etch pits. In addition, a uniform corrosion can be observed as the primary corrosion type, as illustrated in Fig. 2.

According to ISO 8407[22], all specimens were immersed in a hydrochloric acid solution (10%) for 24 hours.After that, the corrosion products were removed by using wire-brush. Using a field emission scanning electron microscope (MERLIN Compact), the surface morphology of two types of specimens, *i.e.* one with natural corrosion followed by de-rusting, and the other with accelerated corrosion followed by de-rusting, were obtained. It was found that surface of

Fig. 1 — Steel tube layout.

these two corrosion samples show the same laminated structure and a similar distribution of etch pits; moreover, the, the surface of morphologies the specimens with corrosion were basically the same, therefore, proving the rationality of the accelerated corrosion experiments methodsapplied. The scanning

results of the specimen surface morphology are shown in Figs 3 and 4.

3 Axial Loading Experiments

3.1 Experiments design

To obtain the axial bearing capacity of the circular steel tubes, axial loading experiments were carried out. Here, a 1000-kN electro-hydraulic servo universal experimenting machine was chosen as the

Fig. 2 — The diagram of steel tubes surface after corrosion.
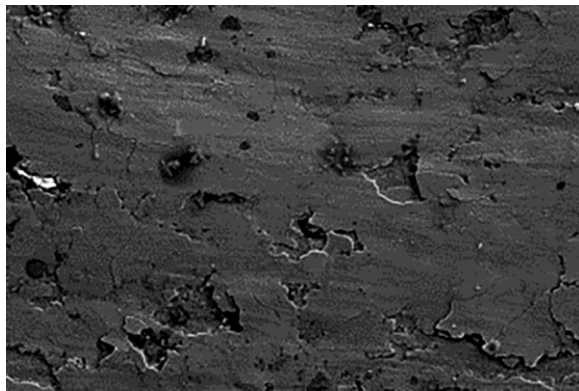
Fig. 3 — The surface morphology of nature corrosion after derusting.
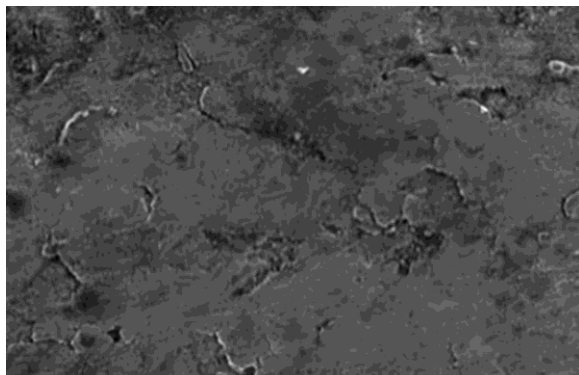
Fig. 4 — The surface morphology of accelerated corrosion after derusting.

loading device, and a statistical strain indicator TST3826-2, Taisite Co., Jiangsu province, was adopted as the strain collection instrument.

Before the experiments, all strain gauges were placed uniformly and symmetrically along the top, centre and bottom sections of the specimens. In addition the four generatrices of the specimen, which were 90 degrees from each other, were numbered clockwise. The gauges were then placed at the intersection points of four generatrices and in three sections, as shown in Fig. 5.

To ensure the forcing of the axial load, the bottoms of the specimens were hinged, and their top and vertical loading ends were fixed. In addition, the entire loading process adopted a hierarchical load system with control. Specifically, a speed of 1kN/s was applied during the early stage until the specimen
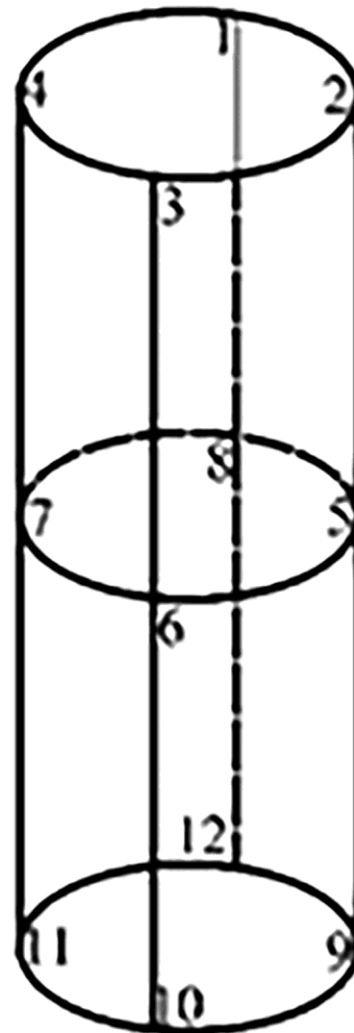
Fig. 5 — Diagram of measuring point layout.

showed plastic characteristics, and when the elastic limit of the specimens was approached, a speed of 0.5kN/s was applied until a failure of the specimen occurred. In the meantime, the strains of specimens were recorded during the loading process. A view of the experiment field is shown in Fig. 6.

3.2 Experimental phenomena

Axial loading experiments on 24 steel tubes in eight groups, marked as A, B, C, D, E, F, G, and H were conducted. Furthermore, the de-rusting process was applied on the surfaces of the corrosive specimens in six groups, namely, B, C, D, E, F and G.

The results indicate that no obvious deformation occurred during the initial loading stage, and the load displacement curve shows nearly a linear trend. With the increase in load, the specimens enter the plastic stage, and the strain increases rapidly, followed by the failure, as indicated in Figs 7 and 8.

After the compressive buckling, bulges appeared at all ends of the specimens in eight groups, which were located at the bottom spherical hinge for specimen

Fig. 6 — Axial loading experiment.
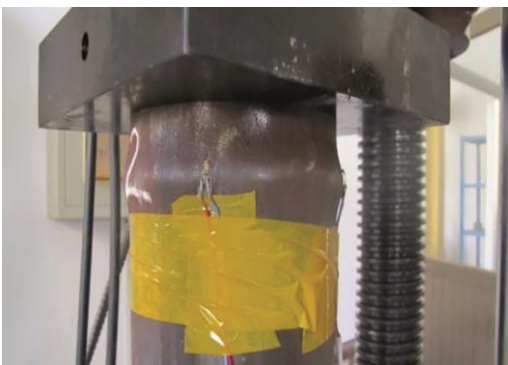
no.3 in group A; no. 2 in group C; all the specimens in group D; specimens with a 89×3 section, indicated as specimen no.2 in group E; no.1 and no. 3in group F; no.3 in group G; and no. 2 in group H, whereas they occured near the loading ends for the remaining specimens. Details of the experiment specimens are shown in Fig. 9.

4 Analysis of Results

4.1 Axial pressure experiment results

Table 3 lists the experiment results of the specimens in the eight groups; where F_{sc} indicates the yield bearing capacities of the tubes, and F_{bc} indicates their ultimate bearing capacities. The load–displacement curves of each specimen are shown in Fig. 10.

Comparing the test results of each group, it was found that uniform corrosion has an effect on the bearing capacity of the circular steel tubes. In addition, with an increase in the degree of corrosion, the ultimate and yield bearing capacities of the steel tube were further reduced. Moreover, it should be noted that, for group D in which the corrosion was the most serious, the yield bearing capacity of the component was very similar to that of the ultimate bearing capacity. This indicates that the components failed rapidly after entering the yield stage. In other words, the safety margin of the components was significantly reduced because of corrosion. It was also found that the corrosion under a corrosion depth of less than 30% had little effect on the failure mode of the components under axial compression.

4.2 Analysis of experiment results

To obtain the relation between degree of uniform corrosion and the bearing capacity of the steel tubes, the weight loss rate D_w of the corrosive steel tubes is taken as an independent variable. In practical

Fig. 7 — Top of destroyed specimen.
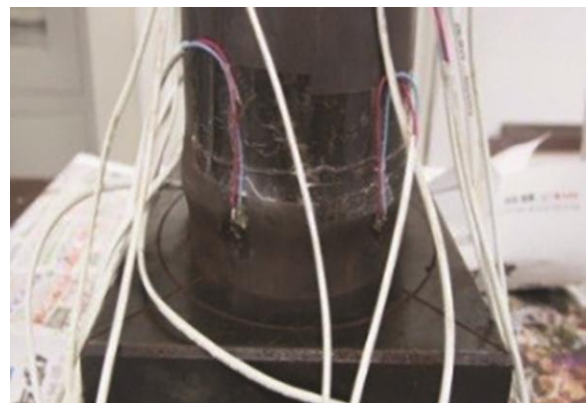
Fig. 8 — Bottom of destroyed specimen.

Fig. 9 — Damage samples from each group.
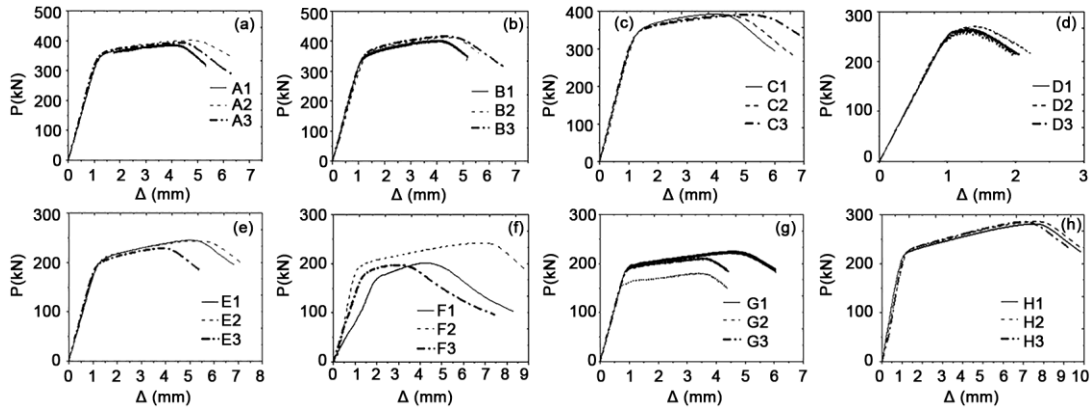
Fig. 10 — Load-displacement curves of experiment.

engineering applications, D_w can be estimated based on the loss in wall thickness. However, the error in the wall thickness measurement is greater than that of the weightlessness measurement. Thus, D_w is widely used in the literature[4, 11, 23, 24]. The measurement of D_w is difficult to achieve under service conditions. However, the mass loss rate can be obtained based on the thicknesses of the original and remaining walls, which can be measured in the structures. The relation between D_w and the bearing capacity can be expressed through Eq. (1) as

$$D_w = (W_0 - W_T) / W_0 \qquad \qquad \ldots(1)$$

where, W_0 indicates the weight of steel tubes before the accelerated corrosion experiments, and W_T is the weight with the de-rusting process applied to the specimen surface (see Fig. 11) prior to the axial loading.

Table 3 shows the weight loss ratio D_w of all specimens. To obtain the relationship between the

Fig. 11 — Before and after de-rusting of no.3 of group D: (a) Before de-rusting, (b) After de-rusting.

bearing capacity and weight loss rate of a corroded steel tube, a linear fitting method was adopted[25]. In addition, the relation between the residual bearing capacities and the weight loss rate of corrosive
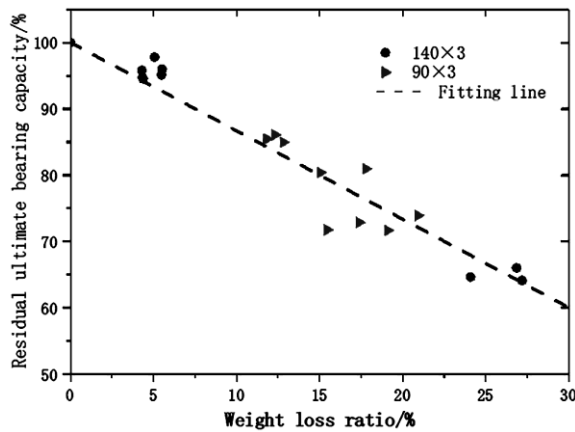
Fig. 12 — Curve of ultimate bearing capacity and weight loss rate.
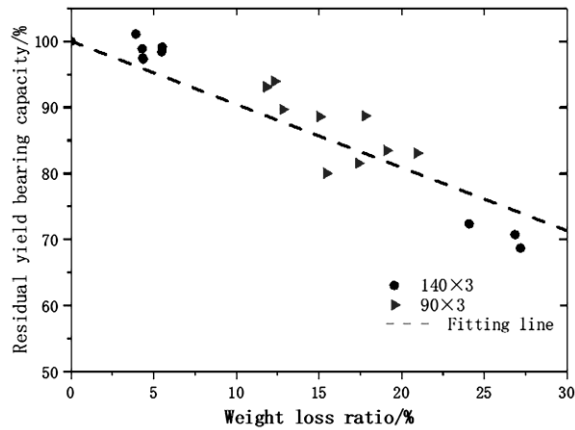
Fig. 13 — Curve of yield bearing capacity and weight loss rate.

Table 4 — Parameter values of fitting formula.

Type	k	Standard error
Ultimate bearing capacity	-1.33	0.046
Yield bearing capacity	-0.95	0.061

circular steel tubes without protective layers can be expressed as:

$$y = 100 - kx \qquad \qquad \dots (2)$$

where y represents the ratio of the bearing capacity of the corrosive specimen to its initial bearing capacity (%), x represents the weight loss rate (%), and k is a fitted parameter.

The results of the linear fitting for the relation of the residual ultimate bearing capacity and weight loss ratio, as well as those of residual yield bearing capacity and weight loss rate, are shown in Figs 12 and 13, respectively. To be precise, the fitted coefficients are as shown in Table 4. The standard
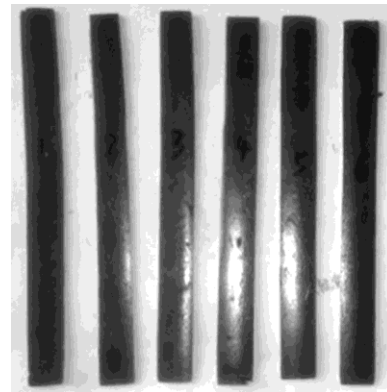
Fig. 14 — Tensile experiment specimens.

errors of the fitted parameter k are 0.046 and 0.061, respectively, which indicate that the fitting effect is good. As Eq. (2) and Table 4 reveal in terms of the relation between the bearing capacity and weight loss ratio, the ultimate bearing capacity is more sensitive to corrosion, and can be instructive to future research and may be applied by researchers for reference.

5 Finite Element Modelling Analysis

To validate the feasibility and accuracy of the finite element (FE) modelling methods applied, the steel tubes used in the experiments were modelled using the shell element (Shell 181) in ANSYS software, and parameters such as the length, diameter, and wall thickness in the tube models complied with the real sizes of the experiment specimens (as indicated in Table 3).

The bilinear kinematic hardening model was selected for simulating the steel. In addition, the material parameters were obtained through material tests in which steel tubes with a length of 200 mm and width of 20 mm, selected from the same batch, were used as the standard specimen for the experiments, as shown in Fig. 14. According to the relevant specifications for a uniaxial tensile experiment[26], the elastic modulus was determined as 193 GPa, the yield strength as 265 MPa, and the ultimate strength as 374 MPa; in addition, the stress–strain curves obtained in the tests are shown in Fig. 15.

The steel tubes used in the test are welded circular steel tubes commonly used in building structures. Longitudinal residual stress caused by welding is likely to affect the bearing capacity of steel tubes. According to the residual stress model proposed by Chen and Ross[27], the residual stress distribution varies significantly with the distance to the weld. The distribution of residual stress is shown in Fig. 16. In
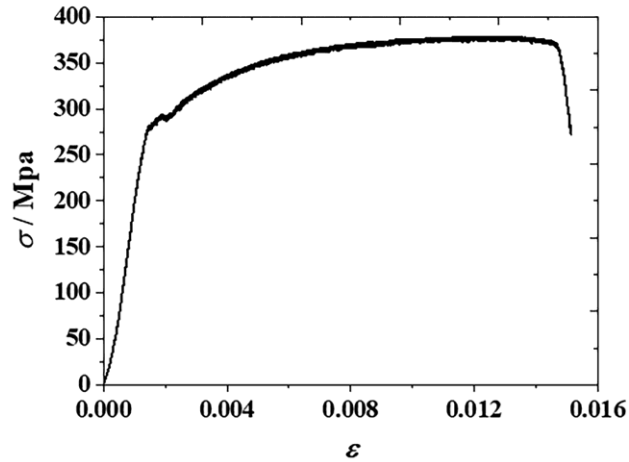
Fig. 15 — Stress-strain curve of steel.
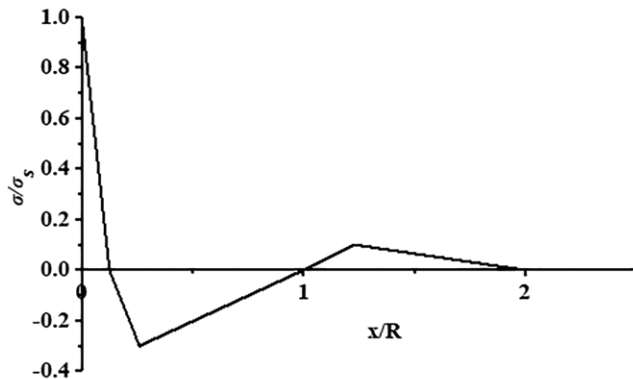
Fig. 16 — Residual stress distribution model.

Fig. 17 — Original ANSYS model of steel tube.
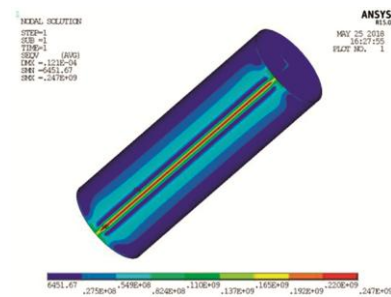
Fig. 18 — Model of the specimen in which residual stress is considered.

addition, the original ANSYS model of a steel tube and a model of a specimen in which the residual stress is considered are shown in Figs 17 and 18, respectively.

In the FE model, the initial geometric imperfections and the residual stress in the material were considered according to the relevant specifications[28]. Because the cross section of the circular tube falls into section category B, the initial value of the deformation at the midpoint of the specimen was selected to be 1/1000, and the deformation at the point with a distance of x to the end was calculated based on the formulas from the specifications.

During the axial compression test, the two ends of the steel tube were unable to move and rotate owing to axial compression. Therefore, the bottom of the specimen in the finite element model was constrained in the radial, circumferential, and vertical directions, whereas the top of the specimen was only constrained in the radial and circumferential directions with free vertical movement. Assuming the corrosion in the specimens to be uniform, the reduction in the equivalent wall thickness of the steel tubes can be considered using their weight loss ratios; that is, the circular steel tubes with varied corrosion depth can be modelled by changing the real constants of the shell element.

The displacement-controlled loading method was utilised in the modelling. During the early elastic loading stage, the applied displacement was relatively large for each loading step. When the stress of the specimen approached its yield strength, the displacement in each step decreased allowing both the descending stage of the loads-displacement curve and the ultimate bearing capacity to be obtained. Table 5 shows the comparison between the values of ultimate bearing capacity from FE modeling and those from the experiments. It can be seen that the results of the ultimate bearing capacity obtained through the experiment and numerical simulation are similar, and most of the deviations are within 10%.

Figure 19 shows the stress–strain curve of the corresponding position of the simulation and experiment from specimen no. 1 in group C. In addition, the deformations of the same specimen, which are from the FE modelling and experiments, are compared in Figs 20 and 21. It was found that the difference in the ultimate bearing capacity during the simulation and experiments is within 15%, except for no. 1 in group F, and that the deformation curves from

Table 5 — Comparison results of ANSYS simulation and experiment.

Grouping	Number	D_w	F_{bc}/kN	F_{bc}^*/kN	F_{bc}^*/F_{bc}
	1	0	403.4	409.3	1.01
Group A	2	0	412.2	407.6	0.99
	3	0	416.6	413.1	0.99
	1	4.37%	388.2	387.3	1.00
Group B	2	5.07%	401.6	384.5	0.96
	3	5.52%	394.2	381.6	0.97
	1	4.30%	393.4	387.2	0.98
Group C	2	4.34%	389.0	387.9	1.00
	3	5.49%	390.6	382.1	0.98
	1	24.08%	265.6	295	1.11
Group D	2	26.85%	271.2	283.1	1.04
	3	27.18%	263.4	281.7	1.07
	1	12.30%	245.0	262.4	1.07
Group E	2	11.82%	243.2	264.1	1.09
	3	15.04%	228.8	251.1	1.10
	1	15.46%	201.4	249.4	1.24
Group F	2	12.80%	241.8	260.1	1.08
	3	17.38%	196.9	233.8	1.15
	1	17.78%	204.0	238.9	1.04
Group G	2	19.09%	230.4	233.4	1.14
	3	20.91%	210.4	228.3	1.09
	1	0	281.4	284.3	1.01
Group H	2	0	286.6	298.9	1.04
	3	0	285.8	298.9	1.05

Here,F_{bc}^* represents the ultimate bearing capacity obtained by finite element simulation
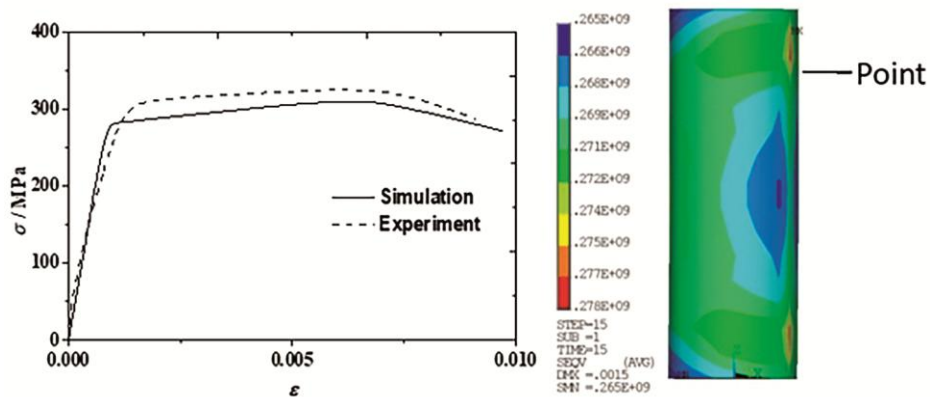
Fig. 19 — Stress-strain curve of finite element simulation and experiment.

the FE modelling and the experiments agree well with each other. Therefore, the corrosion of the circular tubular specimens without a protective layer can be considered as uniform corrosion, and its effect on the bearing capacity of the specimen can be modelled effectively using the FE method with an equivalent reduction in wall thickness.

Finally, to validate the accuracy of the fitting formula for the relation between the ultimate bearing capacity and the weight loss rate of circular steel tubes with uniform corrosion, the ultimate bearing capacities of specimens with a weight loss rate of 5 %, 10 %, 15 %, 20 %, 25 %, and 30 % were obtained through FE modelling, and were compared to the fitted curve of the experiments, as shown in Fig. 22. As can be seen, although the gap between the values of the residual ultimate bearing capacities from the FE modelling and experiments becomes wider with an
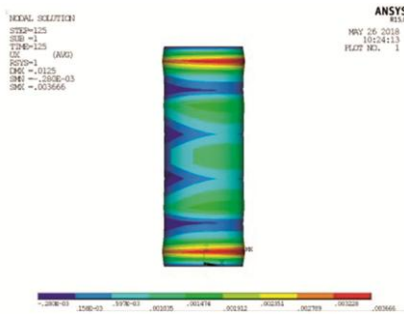
Fig. 20 — Finite element simulation.

Fig. 21 — Experiment example.
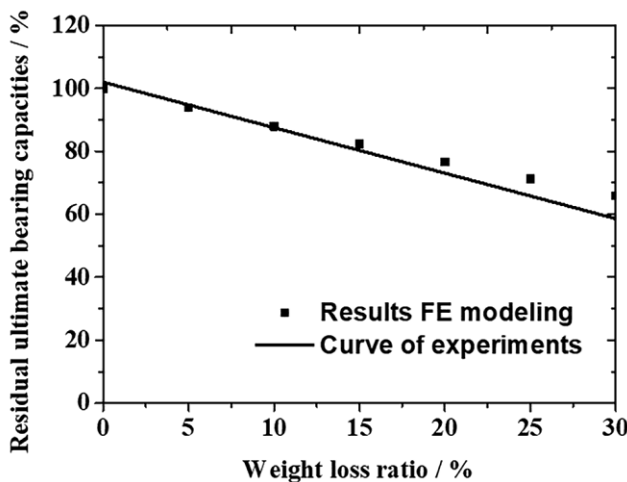
Fig. 22 — Comparison of finite element simulation and experimental curve fitting.

increase in weight loss rate, it is still within 15% when the weight loss rate is below 30%, which validates the reliability of the fitting formula applied.

6 Conclusions

'Utilising accelerated corrosion experiments and the finite element method, the bearing capacity characteristics of corrosive circular steel tubular specimens without protective layers were intensively studied. Herein, the following were discussed:

(i) Complete accelerated corrosion and axial loading experiments on circular steel tubes used in building construction were designed. In addition, a practical modelling method of uniform corrosion for circular steel tubes was proposed, which provides technical reference for research into the mechanical properties of large building components such as circular steel tubes undergoing corrosion.

(ii) The accelerated corrosion and axial loading experiments on the circular steel tube specimens prove that both the yield and ultimate bearing capacities of the components are heavily influenced by corrosion, with the latter being more sensitive. Under uniform corrosion, a good functional relationship exists between the weight loss ratio and the bearing capability of the corroding components. To be specific, the residual bearing capacity ratio is around 80% at a weight loss rate of 15%, and a linear fitting formula depicting the relation between the residual bearing capacity and weight loss rate was proposed based on the experiment data.

(iii) The FE modelling results were shown to agree well with the experiment data, indicating that the corrosion of circular steel tube components without protective layers can be considered as uniform corrosion; this proves the effectiveness of the equivalent strength reduction method in simulating the influence of uniform corrosion on the bearing capacity and verifies the reliability of the fitting formula depicting the relation between the residual bearing capacity and weight loss rate.

References
1   Lener G, Reiterer D & Hauser A, *Procedia Eng*, 66 (2013) 334.
2   Helmerich R, Milmann B & Nussbaumer A, *J Struct Eng*, 125 (1999) 776.
3   João L S, Carvalho R & Fangueiro R A, *Procedia Eng*, 155 (2016) 230.

4 Lee H S & Cho Y S, *Int J Fract*, 157 (2009) 81.
5 Kim Y J, Oh C K & Park C Y, *Int J Pressure Vessels Piping*, 83 (2006) 546.
6 Flaks V Y, *Mater Sci*, 14 (1978) 75.
7 Rahgozar R, *J Constr Steel Res*, 65 (2009) 299.
8 Sharifi Y & Rahgozar R, *Arch Civil Mech Eng*, 9 (2009) 75.
9 Val D V, *J Struct Eng*, 133 (2007) 1297.
10 Stewart M G & Val D V, *J Struct Eng*, 125 (1999) 776.
11 Zhang T, **The Analysis for the Corroded Steel Structure Stiffness and Stability Model** (Xian University of Architecture and Technology, China), (in Chinese), 2015.
12 Pan D & Xu S, *J Water Conservancy Build Eng,* 4 (2009) 57.
13 Teixeira A P, Soares C G, Netto T A & Estefen S F, *Int J Pressure Vessels Piping,* 85 (2008) 228.
14 Caleyo F, González J L & Hallen J M, *Int J Pressure Vessels Piping*, 79 (2002) 77.
15 Amirat A, Mohamed C A & Chaoui K, *Int J Pressure Vessels Piping*, 83 (2006) 107.
16 Rajabipour A & Melchers R E, *Corros Sci*, 76 (2013) 292.
17 Ahn J H, Cheung J H, Lee W H, Oh H & Kim I T, *J Constr Steel Res*, 115 (2015) 290.
18 Netto T, *Appl Ocean Res*, 32 (2010) 132.
19 Oh C K, Kim Y J & Park C Y, *Nucl Eng Des*, 239 (2009) 261.
20 Xiong Z, Guo X, Luo Y, Zhu S & Liu Y, *Thin Wall Struct*, 118 (2017) 124.
21 Zhang C X, Nie G B, Dai J W & Zhi X D, *Eng Fail Anal*, 64 (2016) 85.
22 ISO 8407: 2009, Corrosion of Metals and Alloys—Removal of Corrosion Products From Corrosion Test Specimens, 2009.
23 Garbatov Y, Soares C G, Parunov J & Kodvanj J, *Corros Sci*, 85 (2014) 296.
24 Sheng J & Xia J, *Constr Build Mater*, 131 (2017) 90.
25 Shi W, Tong L, Chen Y, Zigang L I & Kai S, *J Build Struct*, 33 (2012) 53.
26 ASTM A370: Standard Test Methods and Definitions for Mechanical Testing of Steel Products (American Society of Testing Materials, America), 2014.
27 Chen W & Ross D, *Am Soc Civil Eng*, 103 (1977) 619.
28 AISC 360-10: Specification for Structural Steel Buildings, (American Institute of Steel Construction, America), 2010.